AGU PUBLICATIONS

JGR

Journal of Geophysical Research: Solid Earth

RESEARCH ARTICLE
10.1002/2017JB013958

Key Points:
- Earthquake swarms in West Bohemia are not caused by accumulation of crustal stress or by fluid overpressure but by fault weakening
- Fault is repeatedly eroded by fluids due to chemical and hydrothermal fluid-rock interactions and compacted during the swarm activity
- The model of swarm recurrence is supported by observations of accurately determined nondouble-couple components of seismic moment tensors

Supporting Information:
- Supporting Information S1
- Data Set S1
- Data Set S2
- Data Set S3

Correspondence to:
V. Vavrycuk,
vv@ig.cas.cz

Citation:
Vavryčuk, V., and P. Hrubcová (2017), Seismological evidence of fault weakening due to erosion by fluids from observations of intraplate earthquake swarms, *J. Geophys. Res. Solid Earth*, *122*, doi:10.1002/2017JB013958.

Received 9 JAN 2017
Accepted 6 APR 2017
Accepted article online 11 APR 2017

Seismological evidence of fault weakening due to erosion by fluids from observations of intraplate earthquake swarms

Václav Vavryčuk[1] and Pavla Hrubcová[1]

[1]Institute of Geophysics, Czech Academy of Sciences, Prague, Czech Republic

Abstract The occurrence and specific properties of earthquake swarms in geothermal areas are usually attributed to a highly fractured rock and/or heterogeneous stress within the rock mass being triggered by magmatic or hydrothermal fluid intrusion. The increase of fluid pressure destabilizes fractures and causes their opening and subsequent shear-tensile rupture. The spreading and evolution of the seismic activity are controlled by fluid flow due to diffusion in a permeable rock (fluid-diffusion model) and/or by redistribution of Coulomb stress (intrusion model). These models, however, are not valid universally. We provide evidence that none of these models is consistent with observations of swarm earthquakes in West Bohemia, Czech Republic. Full seismic moment tensors of microearthquakes in the 2008 swarm in West Bohemia indicate that fracturing at the starting phase of the swarm was not associated with fault openings caused by pressurized fluids but rather with fault compactions. This can physically be explained by a fault-weakening model, when the essential role in the swarm triggering is attributed to degradation of fault strength due to long-lasting chemical and hydrothermal fluid-rock interactions in the focal zone. Since the rock is exposed to circulating hydrothermal, CO_2-saturated fluids, the walls of fractures are weakened by dissolving and altering various minerals. The porosity of the fault gauge increases, and the fault weakens. If fault strength lowers to a critical value, the seismicity is triggered. The fractures are compacted during failure, the fault strength recovers, and a new cycle begins.

Plain Language Summary The occurrence of earthquake swarms in geothermal areas is usually attributed to a highly fractured rock and/or heterogeneous stress within the rock mass being triggered by magmatic or hydrothermal fluid intrusion. The increase of fluid pressure destabilizes fractures and causes shear-tensile rupture. The spreading and evolution of the seismic activity are controlled by fluid flow due to diffusion in a permeable rock and/or by redistribution of Coulomb stress. This model, however, is not valid universally. We provide evidence that the model is inconsistent with observations of earthquake swarms in West Bohemia, Czech Republic. Microearthquakes in swarms in West Bohemia indicate that fracturing was not associated with fault openings but rather with fault compactions. This can be explained by a fault-weakening model, when the essential role in the swarm triggering is attributed to chemical and hydrothermal fluid-rock interactions in the focal zone. Since the rock is exposed to circulating hydrothermal, CO_2-saturated fluids, the walls of fractures are weakened by dissolving various minerals. The porosity of the fault gauge increases, and the fault weakens. If fault strength lowers to a critical value, the seismicity is triggered. The fractures are compacted during failure, the fault strength recovers, and a new cycle begins.

1. Introduction

Earthquake swarms are seismic sequences clustered in space and time with no distinct main shock and typically observed in volcanic or geothermal areas [*Hill*, 1977; *Scholz*, 2002]. The swarms last from hours to several months comprising thousands of seismic events of magnitude up to 4–5 and occupying a volume of up to several km^3. The swarm activity is attributed to a highly fractured rock and/or heterogeneous stress within the rock mass [*Mogi*, 1963] being triggered by magmatic or hydrothermal fluids [*Hill*, 1977; *Sibson*, 1996]. The role of fluids in generating the earthquake swarms is commonly recognized, and the migration of the activity has often been explained by fluid diffusion in the rock [*Špičák and Horálek*, 2001; *Waite and Smith*, 2002; *Chen et al.*, 2012; *Shelly et al.*, 2013]. Consequently, hydraulic parameters such as fluid pressure, fluid ratio [*Vavryčuk*, 2002], or hydraulic diffusivity and permeability [*Parotidis et al.*, 2005] have been estimated from swarm seismicity in case studies. The important role of fluids in generating swarm activity is further evidenced in fluid-injection experiments [*Baisch and Harjes*, 2003; *Dorbath et al.*, 2009] and in

hydraulic fracturing in oil and gas reservoirs [*Phillips et al.*, 1998; *Baig and Urbancic*, 2010; *Maxwell et al.*, 2010] which induce typical swarm-like microseismicity.

Physically, the mechanism of triggering of the swarm by fluids is explained by the so-called fluid-overpressure (fluid-injection) model. The model assumes an initial fluid intrusion which induces an increase of fluid pressure in a critically organized fracture system [*Bak and Tang*, 1989]. A sudden increase of fluid pressure reduces the effective normal traction on fractures and reduces the critical shear traction needed for failure according to the Mohr-Coulomb failure criterion. Even though the fluid pressure increase does not affect fault strength and friction, it destabilizes the fractures and causes their rupturing. If the fluid pressure is high enough (higher than the minimum compression), pure tensile cracks are formed as, for example, in the hydrofracturing experiments. More often, however, the pressure increase is not so high and fluids just activate predominantly shear cracks with a very small or negligible tensile component. A subsequent spreading and evolution of seismic activity is controlled by fluid flow due to diffusion in a permeable rock (fluid-diffusion model) and/or by the redistribution of Coulomb stress (intrusion model) [*Rubin et al.*, 1998; *Yamashita*, 1999; *Hainzl*, 2004; *Parotidis et al.*, 2005; *Dahm et al.*, 2008; *Shapiro*, 2015]. This process has been modeled numerically by using equations of linear or nonlinear diffusion [*Parotidis et al.*, 2003, 2005; *Miller et al.*, 2004; *Shapiro and Dinske*, 2009] and the epidemic-type aftershock sequence model which describes the statistical properties of sequences when each event can hierarchically produce its own aftershocks [*Hainzl and Ogata*, 2005; *Hainzl et al.*, 2016].

Another physically plausible mechanism of earthquake swarm triggering was suggested by *Heinicke et al.* [2009], who studied a swarm activity in West Bohemia, Czech Republic, and emphasized its close relation to a continuous, long-lasting interaction of fluids with crustal rocks. *Heinicke et al.* [2009] speculate that this interaction leads to an extensive hydrothermal alteration of crustal rocks at focal depth, erosion of faults, and gradual fault weakening, resulting finally in fault failure. A variation of frictional strength of faults caused by fluid migration is also reported by *Yoshida et al.* [2016] for an earthquake swarm in NE Japan. The fault weakening processes are recognized to be important also for standard seismic sequences and can span various time scales. The dynamic fault weakening is reported during a rupture process itself being caused by rapidly elevated pore pressure due to compaction of fluid saturated gouge layer [*Hirakawa and Ma*, 2016] or by thermal pressurization of pore fluids during the seismic slip [*Sibson*, 1973; *Lachenbruch*, 1980]. The long-term fault weakening due to fluid interaction with faults comes from their hydrothermal alteration and involvement of fluids passing through fault-fracture meshes over a broad range of crustal depths. Because of high permeability of faults relative to the host rock, fluids migrate through fault gouge and interact with fault walls [*Sibson*, 2000]. This increases the pore volumes for passing fluids in permeable conduits and promotes the fluid convection. A broader damage zone surrounding the fault core is characterized by porous, highly fractured, and possibly granulated fluid-saturated material. The presence of fluids within a fault zone plays an important role in stability of tectonic faults due to their effect on frictional strength [*Rice et al.*, 2014] and explains weakness of mature faults [*Sleep and Blanpied*, 1992; *Floyd et al.*, 2001].

In this paper, we focus on explaining the origin of intraplate earthquake swarms based on a detailed analysis of earthquake source parameters. We show that the fluid-overpressure model explaining the origin of earthquake swarms is not universally valid being inconsistent with observations of the 2008 earthquake swarm in West Bohemia, Czech Republic. The fluid-overpressure model predicts extensional motions at initial swarm phases due to fault opening by pressurized fluids. These motions are associated with positive nondouble-couple (non-DC) components of seismic moment tensors. Instead, predominantly compressional motions with negative non-DC components are observed at the beginning of the swarm activity. Therefore, we prefer the fault-weakening model for explaining the intraplate swarm's origin and for the earthquake swarm cycle. We support this concept by a careful quantitative analysis of non-DC components of seismic moment tensors and their interpretation in terms of the shear-tensile-compressive source model.

2. The West Bohemia Swarm Area

The West Bohemia/Vogtland region, the border area between the Czech Republic and Germany, is the most seismically active region in the Bohemian Massif [*Babuška et al.*, 2007; *Fischer et al.*, 2014]. It is characterized by persistent seismic activity with frequent occurrence of earthquake swarms. The most prominent earthquake swarms occurred recently in 1985/1986, 1994, 1997, 2000 [*Vavryčuk*, 1993; *Horálek et al.*, 2000; *Fischer and*

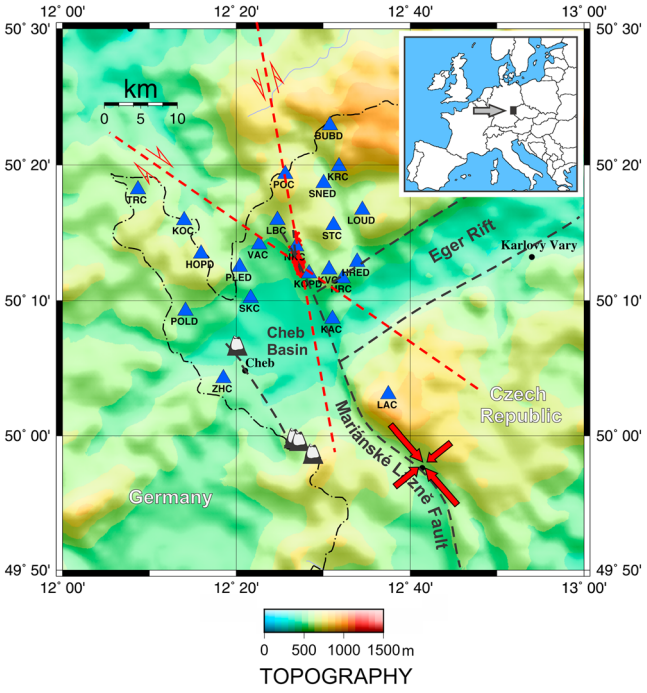

Figure 1. Topographic map of the West Bohemia/Vogtland region. The epicenters of the 2008 swarm earthquakes are marked by red dots. The WEBNET stations are marked by blue triangles. The dashed black lines show the major tectonic lines. The red dashed lines show the orientation of the active faults with strikes of 169° and 304°. The orientations of the maximum and minimum compressions are marked by the full red arrows. The dashed-dotted line shows the border between the Czech Republic and Germany. The cones show four Quaternary volcanoes.

Horálek, 2003], 2008 [*Fischer et al.*, 2010], and 2011 [*Čermáková and Horálek*, 2015] at the same epicentral area called the Nový Kostel focal zone (see Figure 1). The isolated earthquakes as well as earthquake swarms occur also in other areas, but they are significantly less frequent [*Fischer et al.*, 2014]. The duration of the earthquake swarms in the Nový Kostel area was from several days to 3 months, and the activity was focused typically at depths ranging from 7 to 12 km (see Figure 2). The strongest instrumentally recorded earthquake was the M_L 4.6 earthquake on 21 December 1985.

The West Bohemia region is situated in the western part of the Bohemian Massif at the contact of three Variscan structural units: Saxothuringian, Teplá-Barrandian, and Moldanubian [*Babuška et al.*, 2007]. The triple junction of the units is characterized by thinning of the crust with depth of the Moho ranging from 28 km to 32 km [*Hrubcová et al.*, 2013]. The tectonic structure of the area is described by two main fault systems well expressed on the surface: the NW-SE Mariánské Lázně fault system and the SW-NE Ore-Mountain fault system related to Tertiary Eger Rift opening (see Figure 1). However, the recently active fault is the left-lateral strike-slip fault in the N-S direction with a strike of N169°E. This fault forms the eastern boundary of the Cheb Basin filled by Tertiary and Quaternary sediments up to 300 m thick. Another active fault is the right-lateral strike-slip fault in the WNW direction with a strike of N304°E. The seismically active faults not only were identified at depth independently by foci clustering and by focal mechanisms [*Vavryčuk et al.*, 2013] but also have some geological evidence on the surface [*Bankwitz et al.*, 2003]. The left-lateral strike-slip fault was active during the earthquake swarms in 1985/1986 [*Vavryčuk*, 1993], in 2000 [*Fischer and Horálek*, 2003], and in 2008 [*Vavryčuk*, 2011a]. On the contrary, the right-lateral strike-slip fault was active during the earthquake swarm in 1997 and 2008 [*Dahm et al.*, 2000; *Vavryčuk*, 2002, 2011a]. The maximum compressive stress determined from focal mechanisms has an azimuth of N146°E [*Vavryčuk*, 2011a]. This direction coincides well with the average direction N144°E in Western Europe [*Heidbach et al.*, 2008]. The value is slightly rotated with respect to the direction N160°E measured at the KTB superdeep borehole [*Brudy et al.*, 1997], located about 50 km SW of the West Bohemia/Vogtland region. The stress analysis indicates that the two active faults in the region with strikes of N169°E and of N304°E are optimally oriented with respect to the tectonic stress, being the most unstable faults and forming thus a pair of conjugate principal faults in the area [*Vavryčuk*, 2011a]. The deviation of the principal faults from the σ_1 axis is about 32° and corresponds to fault friction of 0.5. This value is slightly less than the value of 0.6–0.8 predicted from laboratory measurements [*Byerlee*, 1978] or the prevailing value of 0.6 observed under geological conditions [*Scholz*, 2002].

Active tectonics is manifested by numerous mineral springs, CO_2 emanations, and Tertiary and Quaternary volcanism (see Figure 3). The massive CO_2 degassing is close to the earthquake swarm area and occurs in the form of CO_2-rich springs and wet and dry mofettes in several degassing fields along the main tectonic fault zones. Contrary to the strike of the faults controlling the earthquake swarms, the band of CO_2

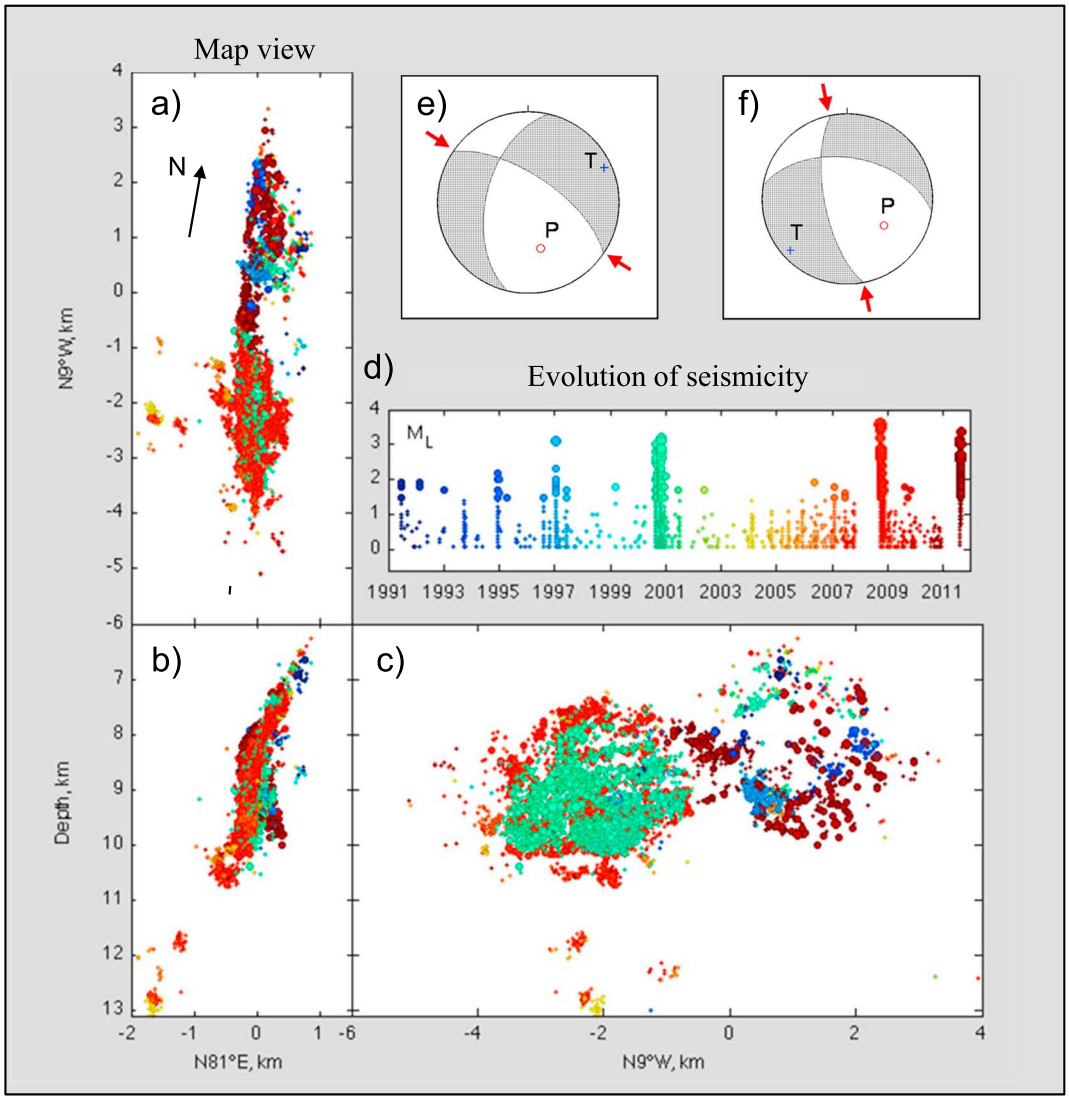

Figure 2. Hypocenters of the seismic activity in the Nový Kostel focal zone for the period from 1993 to 2011 relocated by the (a–c) double-difference method together with the (d) magnitude-time plot and with (e and f) two focal mechanisms characteristic for the focal zone. The locations are shown in the map view (Figure 2a) and in two vertical cross sections (Figures 2b and 2c). The hypocenters are color-coded by the origin time. The fault nodal lines in Figures 2e and 2f are marked by the red arrows. Modified after *Fischer et al.* [2014].

degassing and springs trends NW-SE in the direction of the maximum compressive stress at depth (Figure 1), as well as in the direction of the main fault zones (Marianské Lázně Fault trending NW-SE and the Eger Rift in NE-SW direction). Three main degassing centers (Figure 3) are characterized by high gas flow, high CO_2 concentrations, and high mantle-derived helium contents [*Weinlich et al.*, 1999; *Geissler et al.*, 2005]. In the Cheb Basin, at the intersection of these fault zones, the portion of mantle-derived helium is the highest and the subcontinental helium isotopic signature indicates supplying of magmatic fluids from magma reservoirs at the Moho depths [*Bräuer et al.*, 2008].

3. Earthquake Swarm in 2008

3.1. Seismic Observations

One of the strongest recent earthquake swarms in the West Bohemia region occurred in October 2008 [*Fischer et al.*, 2010; *Vavryčuk et al.*, 2013]. This swarm lasted for 4 weeks being formed by eight distinct phases P1–P8. It involved about 25.000 microearthquakes of magnitudes higher than −0.5 with the largest event

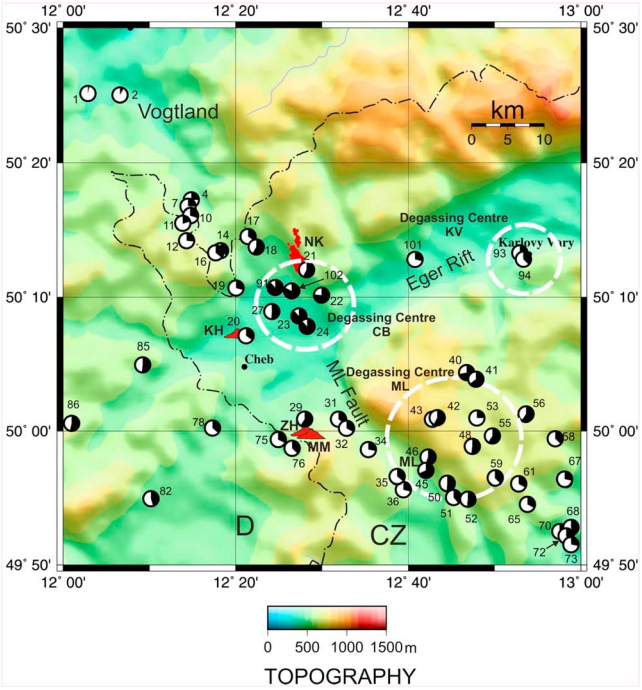

Figure 3. Topographic map of the West Bohemia region with the distribution of degassing locations (small numbers identify the degassing locations after *Geissler et al.* [2005]). The black segments of the circles correspond to the portions of mantle-derived helium ($^3He/^4He \approx 6.5$ *Ra* [*Gautheron et al.* [2005]). The data are taken from *Weinlich et al.* [1999], *Geissler et al.* [2005], and *Bräuer et al.* [2011] (NK = Nový Kostel focal zone, CB = Cheb Basin, ML = Mariánské Lázně, KV = Karlovy Vary). The red dots show the epicenters of 2008 swarm earthquakes, and the red triangles mark Quaternary volcanoes (KH = Komorní Hůrka, ZH = Železná Hůrka, MM = Mýtina Maar). D: Germany, CZ: Czech Republic. After *Fischer et al.* [2014].

reaching the magnitude of 3.8. The epicenters formed a 4 km long cluster striking N170°E. The hypocenters were located at depths of 7.5–11 km. The *b* value of the magnitude-frequency distribution was close to 1.

The swarm was recorded by 22 local three-component seismic West Bohemia Network (WEBNET) stations (Figure 1). The stations have epicentral distance smaller than 25 km and cover the area uniformly with no significant azimuthal gap. Most of the stations are short period with a sampling frequency of 250 Hz and flat frequency response between 1 and 30 Hz. In addition, the station with the nearest epicentral distance (station NKC) was equipped with a broadband STS-2 seismometer. The detection threshold magnitude of the WEBNET network was less than −0.5, and the magnitude of completeness of the earthquake catalogue is about −0.3 [*Fischer et al.*, 2010].

3.2. Locations and Focal Mechanisms

In total, 483 swarm earthquakes recorded at all WEBNET stations were located by *Bouchaala et al.* [2013] in order to analyze a detailed structure of the focal zone. First, initial locations were calculated by the FASTHYPO code [*Herrmann*, 1979] in a layered velocity model of *Málek et al.* [2000] by using manually picked *P* and *S* arrival times. Second, the double-difference relocation method of *Waldhauser and Ellsworth* [2000] was applied to differential times obtained from manual picking as well as from cross correlation in order to increase the accuracy of relative locations. The relative accuracy of the calculated hypocenters within the cluster was estimated to be less than 20 m [*Bouchaala et al.*, 2013]. The accuracy of the absolute location of the cluster is about 100 m in the horizontal plane and 350 m in depth [see *Bouchaala et al.*, 2013].

Accurate locations of the 483 swarm earthquakes indicate that individual swarm phases activated different patches on the fault (see Figure 4). The swarm activity started at depths of 10.5–11.0 km and gradually moved to shallower depths. The last swarm phase P8 activated a fault segment at depths of 7.5–8.5 km (see Figure 4c). A detailed migration of foci of the first three swarm phases P1–P3 (see Figure 4d) reveals that the foci systematically move upward along the fault, from depths of 11.0 km in the south to depths of 7.5 km in the north. The N-up movement coincides with the rake of −40° to −50° typical for the predominant left-lateral strike-slip focal mechanism (except for the orientation). Later phases P4–P8 are shallower than phases P1–P3 but with no further shift to the north.

The microearthquakes form typically multiplets (see Figure 5). The focal mechanisms of microearthquakes are of two basic types (see Figure 6): the left-lateral strike slips (mechanism A, ϕ = 169°) with a weak normal component and the right-lateral strike slip (mechanism B, ϕ = 304°) with a normal component. The left-lateral strike slips are prevailing being scattered over the whole focal area. The two basic types of the focal mechanism are called the principal focal mechanisms because the fault segments associated with them are optimally oriented with respect to the tectonic stress in the region [*Vavryčuk*, 2011a]. A small portion of events display

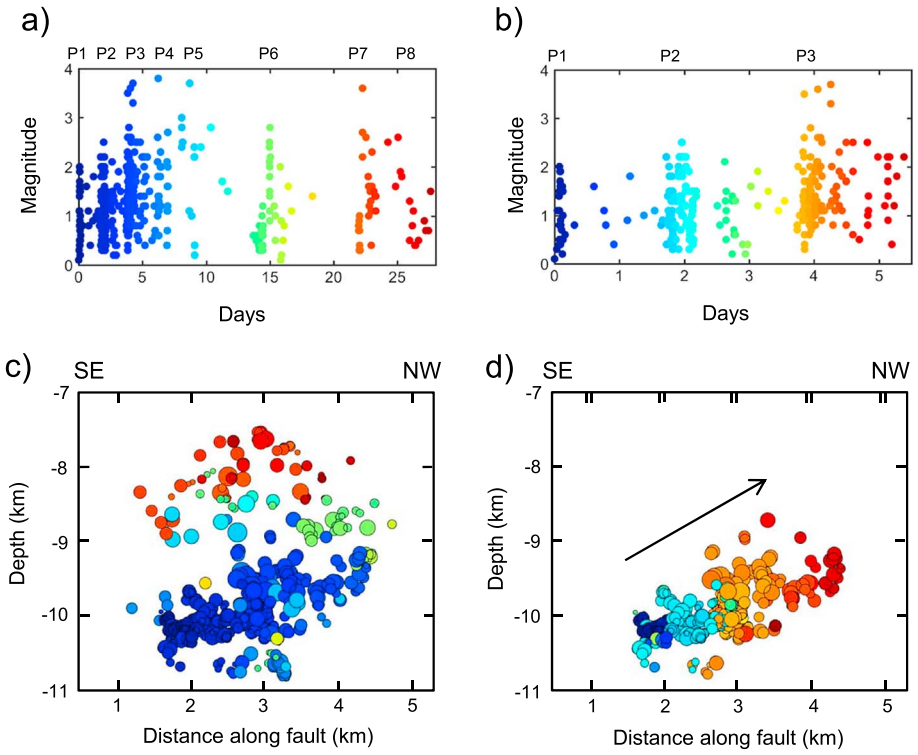

Figure 4. Migration of foci of 483 selected swarm earthquakes. Magnitude-time plot for the whole period of the (a) swarm and for the (b) first three swarm phases. Foci of earthquakes projected on the fault for the whole period of the (c) swarm and for the (d) first three phases. The foci are color-coded according to their origin time and scaled according to their magnitude. The color-coding is consistent for plots showing the same time period: for Figures 4a–4c and for Figures 4b–4d. The arrow in Figure 4d marks the direction of foci migration. The direction of the slip is for the typical focal mechanisms (with strike/dip/rake of 170°/75°/−40°) parallel to the arrow direction but aiming downward.

also some other focal mechanisms associated with small patches in the focal area. These patches indicate the existence of several differently oriented small-scale fault segments [*Vavryčuk et al.*, 2013].

3.3. Inversion of Focal Mechanisms for Stress

In order to understand faulting processes during the swarm activity, stress conditions in the focal area and tractions acting on individual fault segments should be known. *Vavryčuk* [2011a] and *Vavryčuk et al.* [2013] studied the focal mechanisms of the 2008 earthquake swarm and inverted them for stress. They found that the pressure (P) and tension (T) axes are well clustered and form the so-called butterfly wings. Stress in the focal area was also inverted by *Vavryčuk* [2014] who applied the stress inversion of *Michael* [1984, 1987] improved by incorporating the fault instability criterion for resolving the ambiguity of focal mechanisms and distinguishing the fault from the auxiliary nodal plane. The resultant principal stress directions (azimuth/plunge) are as follows [*Vavryčuk*, 2014, Table 1]: σ_1 = 139°/35°, σ_2 = 332°/54°, and σ_3 = 233°/7°. The stress ratio R is 0.78. The corresponding two principal focal mechanisms are (strike/dip/rake) 164°/81°/−37° and 298°/66°/−149°. The errors in the stress directions and stress ratio R are about 6° and 6%, respectively. The stress analysis indicates that the majority of the activated fractures are well oriented for shear faulting.

4. Moment Tensors of Swarm Earthquakes in 2008

4.1. Inversion Method

The moment tensors (MTs) of the data set under study were calculated through the inversion of *P* wave amplitudes. This inversion proved to be an efficient and accurate method for determining MTs of micro-earthquakes recorded by local seismic stations [*Šílený*, 2009; *Horálek et al.*, 2010; *Pesicek et al.*, 2012; *Stierle et al.*, 2014]. Since amplitudes of the direct *P* wave are inverted, the method is less sensitive to

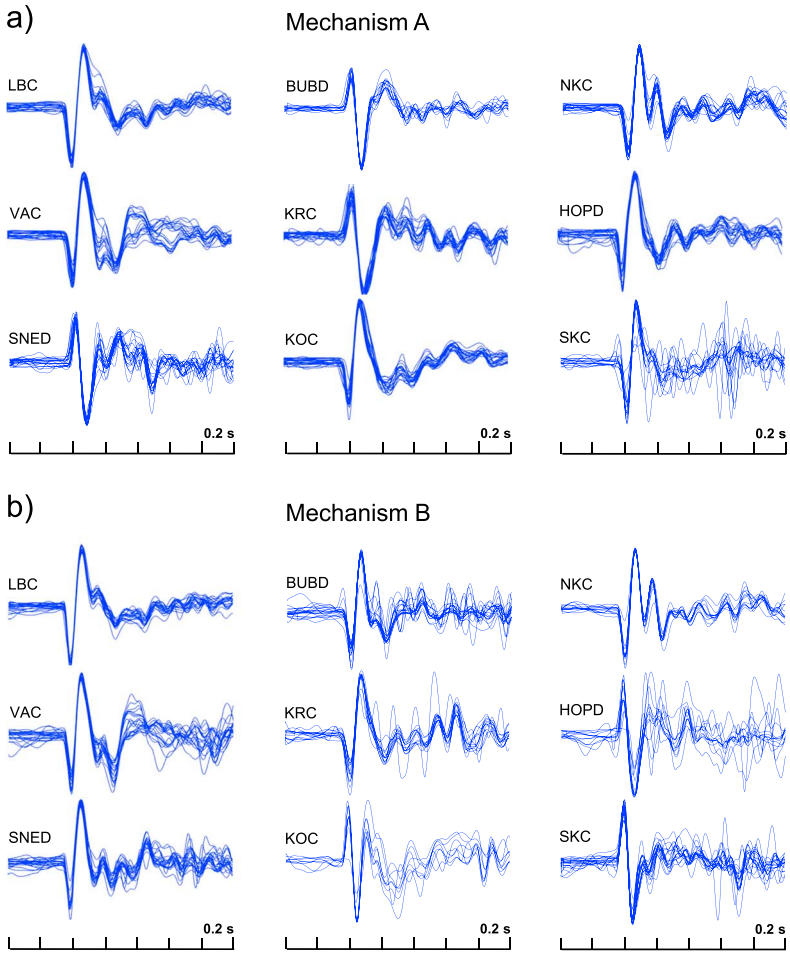

Figure 5. *P* waveforms of two sets of 20 microearthquakes characterized by (a) left-lateral oblique strike slips (mechanism A) and (b) right-lateral oblique strike slips (mechanism B). The waveforms are normalized to their maximum amplitude. The waveforms manifest (1) their simple structure with a predominant direct *P* pulse and (2) their similarity typical for multiplets. The vertical components of displacement are shown for nine stations of the WEBNET network.

unknown crustal small-scale inhomogeneities and to crustal anisotropy producing coda waves and shear wave splitting, respectively. Both types of structural complexity are often mismodeled in waveform inversions, so that they deteriorate fitting of synthetic and complete waveforms and reduce the accuracy of the resultant MTs [*Šílený and Vavryčuk*, 2000, 2002]. This difficulty typical for high-frequency waveforms of local microearthquakes or for regional earthquakes with an unknown velocity model is often overcome by inverting individual phases extracted from full waveforms [*Zhao and Helmberger*, 1994; *Nayak and Dreger*, 2014; *Alvizuri and Tape*, 2016] and thus emphasizing information on amplitude of the phases in the inversion.

The analyzed data set consists of the 483 swarm earthquakes accurately located by *Bouchaala et al.* [2013]. The set comprises events with magnitudes ranging from 1.0 to 3.8 and covers the entire focal zone and the whole variety of focal mechanisms. The velocity records were integrated into displacement and band pass filtered in the frequency range of 1–25 Hz to suppress seismic noise (see Figure 5). The predominant frequencies of the signal were mostly between 5 and 15 Hz. The amplitudes of the direct *P* wave were measured by an analyst and inverted for full moment tensors. The Green's functions, as a response of the medium, were computed by using the ray method [*Červený*, 2001]. We used a 1-D gradient velocity model obtained by smoothing the layered model used for locations. In order to get accurate moment tensors, the measured amplitudes were corrected for amplification factors obtained by the so-called network calibration proposed by *Davi and Vavryčuk* [2012]. Inverting the whole data set of earthquakes, the method is

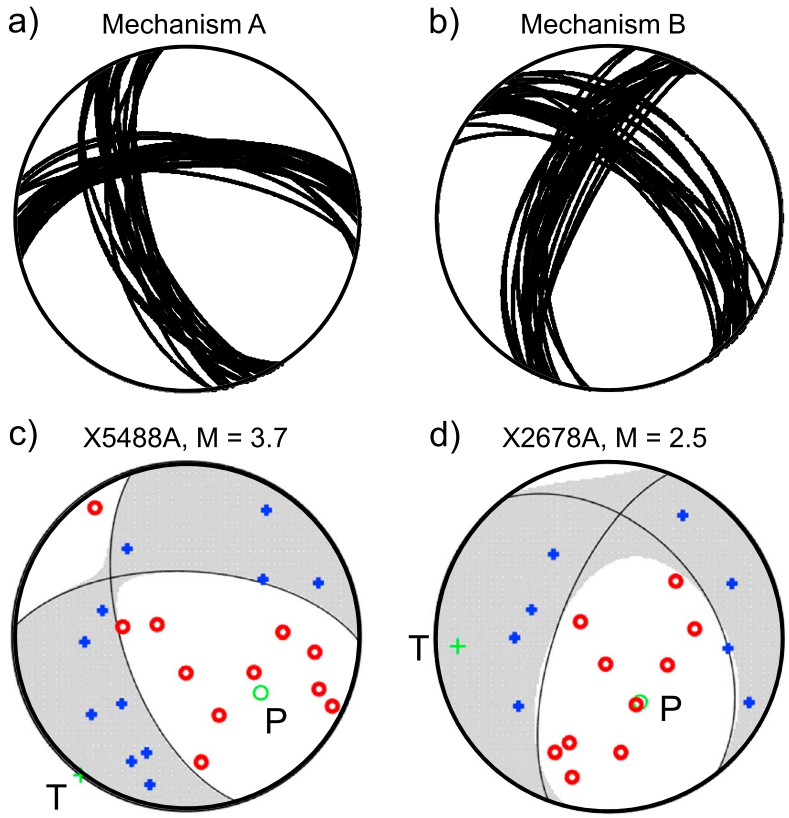

Figure 6. Focal mechanisms of two sets of 20 multiplets from Figure 5 with (a) mechanism A and (b) mechanism B together with examples of focal mechanisms for two individual events: (c) event X5488A of 14 October 2008 at 19:00:33 with M_L = 3.7 and (d) event X2678A of 10 October 2008 at 16:20:35 with M_L = 2.5. The blue plus signs and red circles in Figures 6c and 6d mark the positive and negative polarities of *P* waves recorded at the WEBNET stations, respectively.

capable to correct the Green's function for unknown site effects or for other local inhomogeneities not included in the velocity model. The full moment tensors are obtained by using the generalized linear inversion and decomposed into the double-couple (DC), isotropic (ISO), and compensated linear vector dipole (CLVD) components [*Vavryčuk*, 2002, 2015].

4.2. Uncertainties of Non-DC Components

The retrieved MTs are of an unprecedentedly high accuracy (see Data Set S1 in the supporting information). This was achieved by inverting data (1) with a high signal-to-noise ratio, (2) with simple waveforms with dominating direct *P* wave indicating absence of strong crustal heterogeneities or anomalous site effects (see Figure 5), and (3) recorded at a large number of local stations at small epicentral distance and with dense and uniform coverage of the focal sphere (see Figures 6c and 6d). The reliability of the MTs was assessed by the root-mean-square residuals (RMS) between the synthetic and observed amplitudes. In addition, the accuracy was estimated by multiple inversions of amplitudes contaminated by random noise of uniform distribution with a noise level up to 20%. The foci were mislocated with an error of 250 m in the epicenter and of 500 m in depth. The velocity model was perturbed with velocity perturbations of 5%. Based on these tests, we selected 249 earthquakes recorded at least at 15 local stations with the most reliable MTs characterized by the RMS less than 0.20, by the standard errors in the strike, dip and rake angles less than 5°, and by the standard errors in the ISO and CLVD less than 3 and 8%, respectively.

Note that the percentages of the ISO and CLVD are mutually independent, their trade-off being reduced to minimum. This trade-off appears when the CLVD axis is nearly vertical, and thus, the radiation patterns of the ISO and CLVD are similar. This is eliminated for our data because the CLVD axis for the majority of events is along the T axis, which is nearly horizontal (see Figures 6c and 6d).

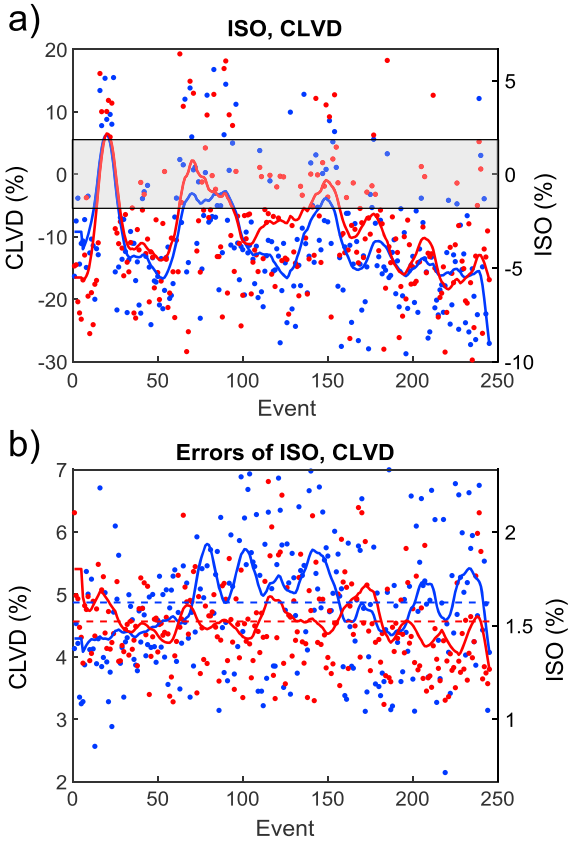

Figure 7. (a) The CLVD (blue) and ISO (red) components of 249 selected moment tensors. (b) The standard deviations of the CLVD (blue) and ISO (red) components. The order of events is according to their origin time. In order to better visualize the CLVD-ISO correlation, the scales of the CLVD and ISO components differ by a multiplication factor of 3. The dashed area in Figure 7a denotes the error limits for the CLVD and ISO produced by inaccuracies in the inversion of the DC moment tensors. The blue and red dashed lines in Figure 7b show an average error of the CLVD and ISO components, respectively. The CLVD and ISO percentages are calculated by using the formulas of *Vavryčuk* [2015, equations (6–9)].

4.3. Basic Characteristics of Non-DC Components

Figure 7 shows the values of the CLVD and ISO components for the 249 most accurate moment tensors together with moving averages calculated over moment tensors of 10 successive analyzed earthquakes depicted according to their origin times. Apparently, the averaged curves smooth the scattered values of the CLVD and ISO components. The scatter has the two following origins:

1. The scatter is partly due to the errors of the MT inversion. The standard deviations of the ISO and CLVD are less than 3 and 8% for all selected moment tensors (see Figure 7b). The mean ISO and CLVD standard deviations are of 1.5 and 5.0%, respectively (see Figure 7a, shadow area, and Figure 7b, dashed lines). Since the ISO and CLVD are out of the error limits for most of the events, the major part of the non-DC components cannot be explained by the inversion errors.
2. The scatter can reflect random nature of physical processes at the focal area caused by irregularities of the fault geometry, of strength distribution along the fault, and of space-time distribution of stress.

Calculating the moving average of the non-DC components, we can suppress the scatter of the non-DC components (of either numerical or physical origin) and enhance systematic variations and trends. These variations should primarily be caused by physical conditions and processes in the source, such as tensile/compressive faulting or seismic anisotropy in the focal area [*Vavryčuk et al.*, 2008].

5. Interpretation of Non-DC Components

The non-DC components consist of the isotropic (ISO) and the compensated linear vector dipole (CLVD) components. They might be spurious being produced by numerical errors of the inversion, when the amount of data is limited, by the inaccuracy of the Green functions, or by the inadequate simplification of the source process [*Šílený et al.*, 1996; *Panza and Sarao*, 2000; *Šílený*, 2009]. The dense station configuration, good azimuthal coverage, and high-quality observations in West Bohemia, however, do not support this interpretation and favor their physical origin [*Frohlich*, 1994; *Julian et al.*, 1998; *Foulger et al.*, 2004]. The most common physical mechanisms producing non-DC components are seismic anisotropy, tensile/compressive faulting [*Vavryčuk*, 2005, 2011b; *Vavryčuk et al.*, 2008], or collapses in mines [*Rudajev and Šílený*, 1985; *Šílený and Milev*, 2008; *Trifu and Shumila*, 2010; *Kuehn and Vavryčuk*, 2013; *Whidden and Pankow*, 2016]. Anisotropy in the focal area can produce ISO and CLVD components even for shear faulting. In this case, the ISO and CLVD are, in general, uncorrelated and depend on the orientation of faulting with respect to anisotropy

axes [*Vavryčuk*, 2005]. Consequently, the variations of the ISO and CLVD in anisotropic media reflect variations of the focal mechanisms. By contrast, the ISO and CLVD in the 2008 West Bohemia swarm are well correlated, and the focal mechanisms do not display any systematic time variations which could explain the time dependence of the ISO and CLVD in Figure 7a. The ISO and CLVD vary even for earthquakes with identical focal mechanisms. For these reasons, we can conclude that the anisotropy effects should not be dominant and the most plausible origin of the observed non-DC components is tensile (or compressive) faulting.

5.1. Shear-Tensile-Compressive Source Model

Real physical non-DC components of the moment tensors observed in geothermal areas are usually produced by tensile faulting associated with the presence of fluids [*Kravanja et al.*, 2000; *Panza and Sarao*, 2000; *Vavryčuk*, 2002; *Foulger et al.*, 2004]. Injection of pressurized fluids can open the fault, while leakage of fluids can close the fault. In both cases, the slip vector does not lie in the fault and nonshear faulting is observed. Mathematically, this rupture process is described by the so-called shear-tensile-compressive source model or simply the tensile model [*Vavryčuk*, 2011b]. The model is defined by the orientation of the normal **n** to the fault (fracture) and by the slip vector **u** with moment tensor **M** expressed in isotropic media as [*Vavryčuk*, 2005, equation (4)]:

$$M_{ij} = \lambda S n_k u_k \delta_{ij} + \mu S \left(n_i u_j + n_j u_i \right), \tag{1}$$

where λ and μ are the Lamé's coefficients and S is the fracture size.

The deviation between the slip vector and the fracture plane is called the slope angle α (see Figure 8). For shear faulting, α is zero and the moment tensor is pure DC. Positive values of α correspond to fault opening (Figure 8a) and produce positive ISO and CLVD. Negative values of α correspond to fault closing (Figure 8b) and produce negative ISO and CLVD. The slope angle is calculated from the eigenvalues of the moment tensor, M_1, M_2, and M_3 [*Vavryčuk*, 2011b, equation (18)]:

$$\sin\alpha = \frac{M_1 + M_3 - 2M_2}{M_1 - M_3}, \tag{2}$$

where $M_1 > M_2 > M_3$.

5.2. CLVD, ISO, and Slope Angle

As shown in Figure 8, the model of tensile faulting is characterized by a linear dependence between the ISO and CLVD components. This dependence is detected also in the observed data (see Figures 9a and 9b). The correlation coefficient between the observed ISO and CLVD (Figure 7a) attains a value of 0.83, indicating that the model of tensile faulting adequately describes the fracture process in the focal zone. In addition, the predominantly negative values of the ISO and CLVD point out to mainly compressive faulting, when the slope angle is negative and the fault is closing during the seismic activity (see Figures 9a and 9b).

Figure 9c shows the histogram of the slope angle calculated for the analyzed events by using equation (2). The slope angles range between $-20°$ and 10° with most frequent values between $-7°$ and $-5°$. The uncertainty of the slope is estimated similarly as for the CLVD and ISO by multiple MT inversions of amplitudes contaminated by random noise of uniform distribution with a noise level up to 20%. The slope error calculated as the mean standard deviation of slopes calculated from noisy MTs and averaged over all earthquakes is 4°. Since the slope of the majority of earthquakes is out of the error limits of shear faulting (see Figure 9c), it cannot be an artifact of the inversion but should reflect nonshear nature of faulting. In addition, systematic variations of the slope evaluated for consecutive earthquakes indicate evolution of faulting regime in time, as discussed in the next section.

5.3. Time Variation of Slope

The time evolution of prevailing fracture mode in the focal zone can be traced by variation of the slope angle of earthquakes in time. To enhance systematic variations we calculate the moving average of the slope over 10 successive earthquakes similarly as in the analysis of the ISO and CLVD components (see Figure 7) and plot it as a function of time (see Figure 10). As seen in Figure 10, the slope angle exhibits clear time variations correlated with the activity rate during the swarm.

The most prominent changes are observed during the first 5 days of the swarm (see Figure 10c) which are densely covered by the analyzed earthquakes. This time period comprises three distinct phases of the

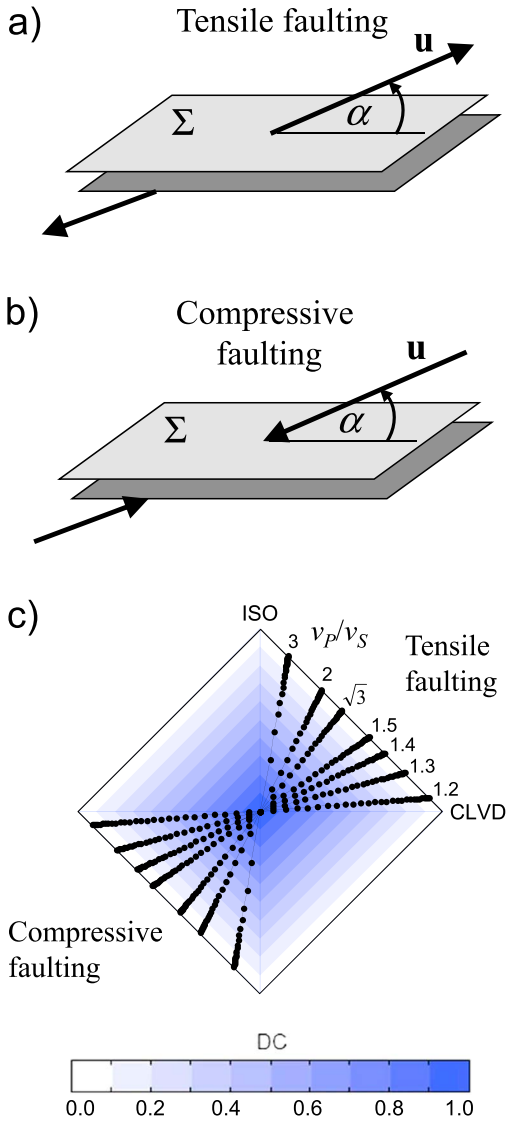

Figure 8. Model of (a) shear-tensile and (b) shear-compressive faulting and the (c) corresponding source-type plot. The angle α between slip vector **u** and fault plane is the slope. (c) The dots correspond to the sources with specific values of the slope angle and the v_P/v_S ratio. The slope angle ranges from −90° (pure compressive crack) to 90° (pure tensile crack) in steps of 3°. The dots form lines with orientation controlled by the v_P/v_S ratio of the medium in the focal zone. The values of the v_P/v_S ratio are indicated in the plot. The plot is color-coded according to the percentage of the DC. The pure shear events (DC = 1, α = 0°) are located in the center of the diamond. Pure tensile and compressive events (DC = 0, α = ±90°) are located at the boundary of the diamond.

swarm activity P1–P3. The beginning of the phases is characterized by an abrupt decrease of the slope angle to negative values of −5° to −10° corresponding to mixture of shear-compressive fracturing. After that, the slope angle continuously increases attaining zero or even positive values (namely the period after P1). The periods of distinct shear-compressive fracturing vary for individual swarm phases.

In order to assess the reliability of the time variation of the slope by using moving averaging we perform additional numerical tests. First, we calculate the time variation of the slope by moving averaging over 6 and 16 successive earthquakes, respectively (Figures 11a and 11b). Again, the abrupt drop of the slope angle at the beginning of the individual swarm phases is clearly visible. Obviously, strong smoothing in Figure 11b reduces the range of slope variations and suppresses their details. As a consequence, the slope anomalies associated with phase P1 and with the follow-up activity are suppressed because this period is short and covered by a rather low number of earthquakes. Nevertheless, the basic properties of the slope variation are conserved for all moving average windows (see Figures 10c and 11a and 11b). Second, we estimate uncertainties of moving averaging due to the errors of the slope of individual earthquakes. We superimpose Gaussian noise with the standard deviation of 4° to slopes of individual earthquakes and calculate 100 moving average curves. The scatter of the curves determines the standard deviation σ. The uncertainty limits are alternatively defined by 1σ and 2σ. Figure 11 shows that compressive faulting regime in swarm phases P1–P3 is significant for both kinds of uncertainty limits and for both moving average windows.

6. Origin of Earthquake Swarms in West Bohemia

The standard model for repeating occurrence of earthquakes is based on the assumption that stress is gradually accumulated in the Earth's plates due to plate motion, and when the stress exceeds a critical

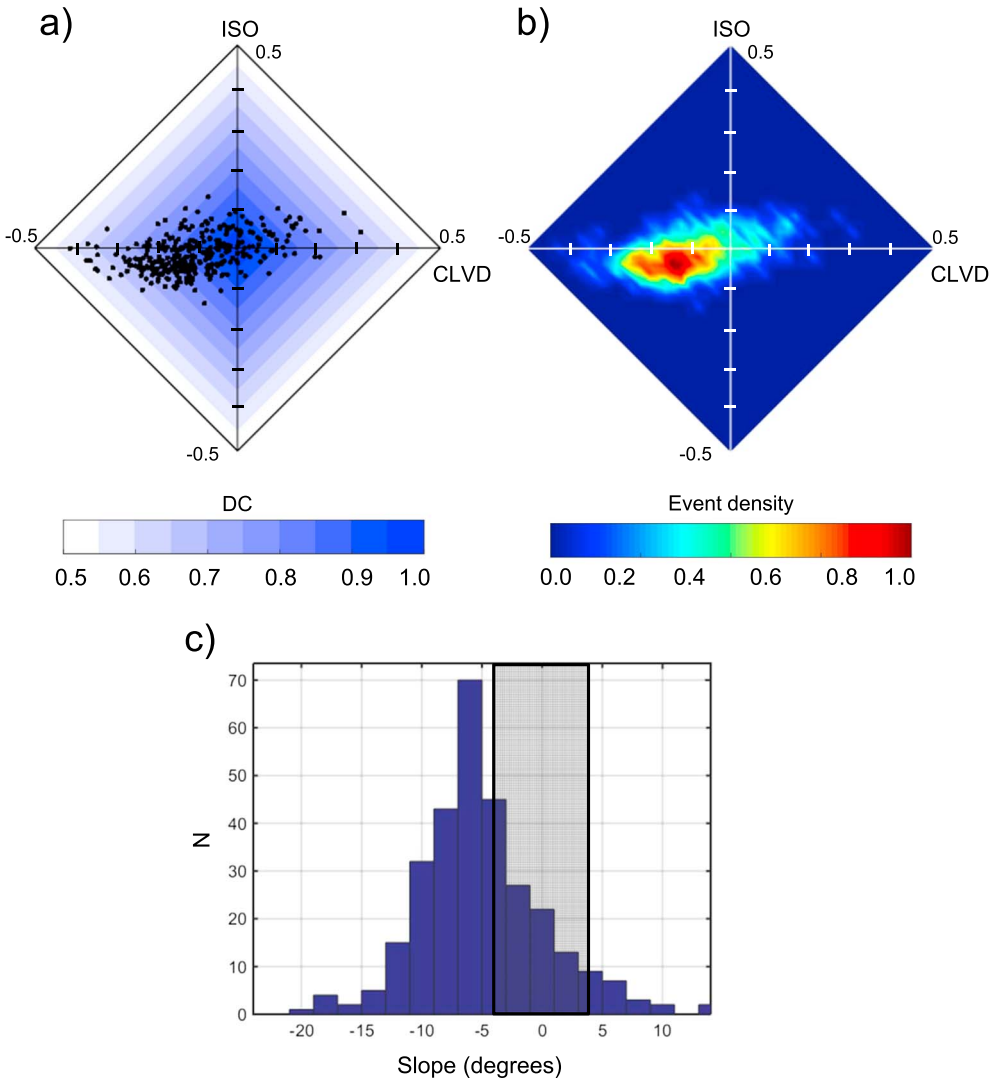

Figure 9. Non-DC components of 249 selected moment tensors. (a) The diamond CLVD-ISO plot showing non-DC components of individual earthquakes. (b) The diamond CLVD-ISO plot showing the density of non-DC components of earthquakes. (c) Histogram of the slope angles calculated from eigenvalues of moment tensors by using equation (2). The red color in Figure 9b indicates the non-DC components for the majority of earthquakes. In order to increase the resolution of Figures 9a and 9b the plots are normalized to the maximum CLVD and ISO values of 50%. The event density in Figure 9b is normalized to its maximum value. The shaded area marks the error limits produced by inaccuracies in the inversion of the DC moment tensors. Figure 9a was plotted by using the open-access Matlab code MT-DECOMPOSITION (http://www.ig.cas.cz/mt-decomposition).

strength of the fault, an earthquake occurs [*Kanamori and Brodsky*, 2004]. The stress is then relaxed, and a new earthquake cycle begins. This explains seismicity at plate boundaries but not the origin of intraplate seismicity where a dominant role of plate motion in building the tectonic stress is lost.

6.1. Fluid-Overpressure Model

The earthquake cycles of intraplate earthquake swarms can be explained by the presence of steady state fluid flow or fluctuating fluid injection from depth into a focal zone where fluids are captured with no escape due to impermeable rocks. When fluids accumulate in the rock they can build overpressure. If the fluid pressure reaches a critical value, the seismic activity is triggered (see Figure 12a). Hence, the seismicity is not initiated by reducing fault strength but by reducing the normal traction on the fault by high pore fluid pressure. The fractures are opening during failure and forming paths for fluids leaving the focal area. Once the fluid pressure drops and the fractures seal, a new cycle begins. The fluid-overpressure model predicts moment

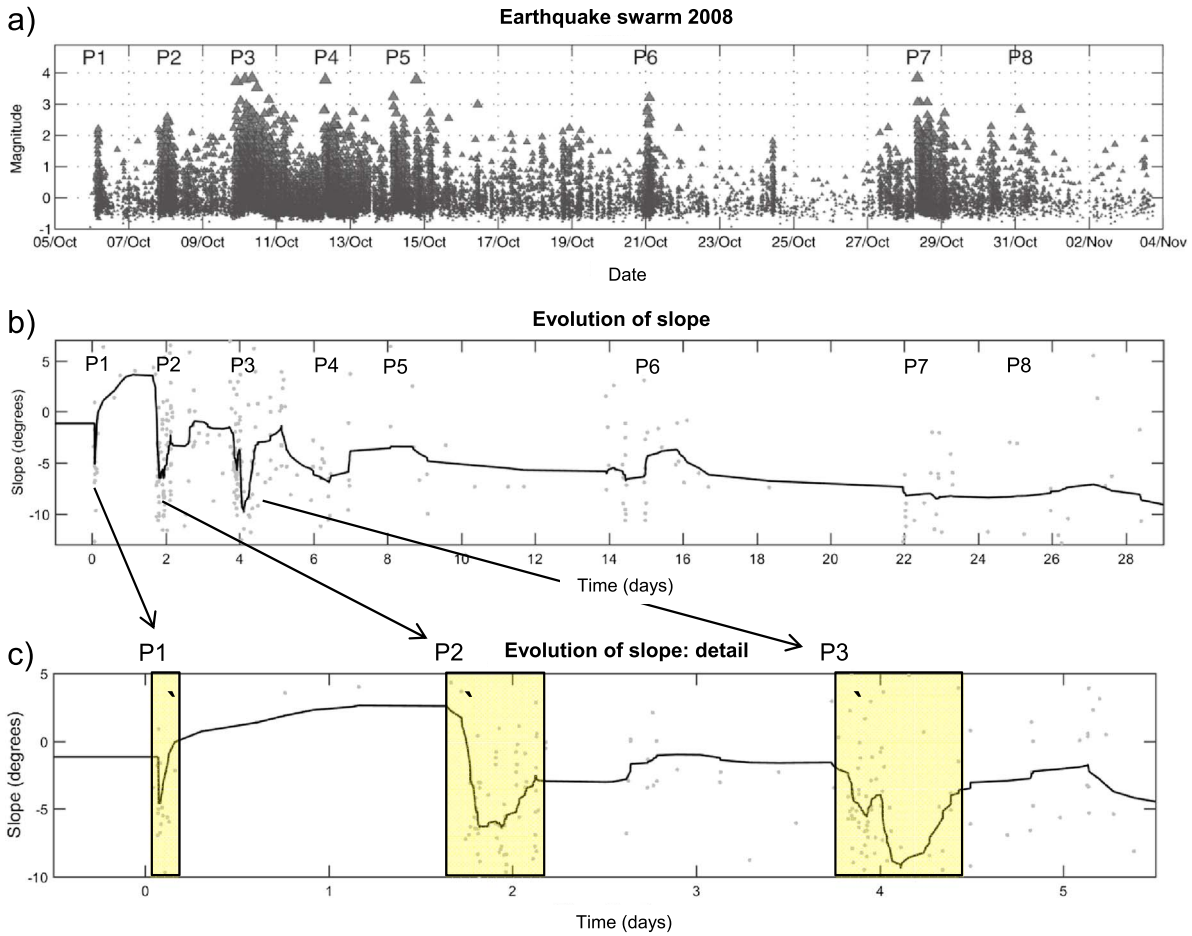

Figure 10. Evolution of seismicity of the 2008 earthquake swarm. (a) Magnitude-time plot for earthquakes with magnitude higher than −0.5. (b) The slope angle as a function of time. (c) Detailed time evolution of the slope for the first three swarm phases of the 2008 earthquake swarm. The phase numbers P1–P8 of the swarm are indicated at the top of plot Figure 10a. The gray dots in Figures 10b and 10c show slopes for 249 selected earthquakes; the solid lines show the moving averages over slopes of 10 successive earthquakes. The yellow rectangles in Figure 10c denote the individual swarm phases P1, P2, and P3 with a significant drop in the slope angle.

tensors with zero or positive non-DC components. Tensile faulting is observed, in particular, at the very beginning of the seismic swarm when the activated fractures are opened due to fluid overpressure. The amount of the positive non-DC components depends on the sudden fluid pressure increase. If it is high enough, pure tensile cracks can be formed. If it is not so high, predominantly shear cracks with a small or negligible tensile component will be activated. Since the non-DC components of the moment tensors of the 2008 swarm in West Bohemia do not support these predictions, such a mechanism is not plausible in this case.

6.2. Fault-Weakening Model

The observation of negative non-DC components of moment tensors at the beginning of the swarm activity points to a rather different physical mechanism of the swarm triggering. Instead of fracture opening during shear-tensile faulting, fracture compaction is observed, indicating the shear-compressive faulting. This can be explained by a process when the rock is exposed to circulating hydrothermal, possibly CO_2-saturated, fluids, which act aggressively on the host rock by dissolving and altering its minerals. The fractures serve as major paths for fluid flow in the crust from depth to surface. They are eroded at a high rate in contact with a steady state flow of the acid fluid phase, and the stressed fault zone is gradually weakened by hydrothermal alteration [*Heinicke et al.*, 2009]. According to *Heinicke et al.* [2009], the expected temperatures at hypocenter depths of 5–12 km range between 130 and 350°C, at a minimum hydrostatic pressure of 0.5–1.2 kbar. These *P-T* conditions appear optimal for the alteration process of granites or metamorphic rocks as proved in experiments [*Suto et al.*, 2007]. The alteration processes of the host rock can also be recognized in the

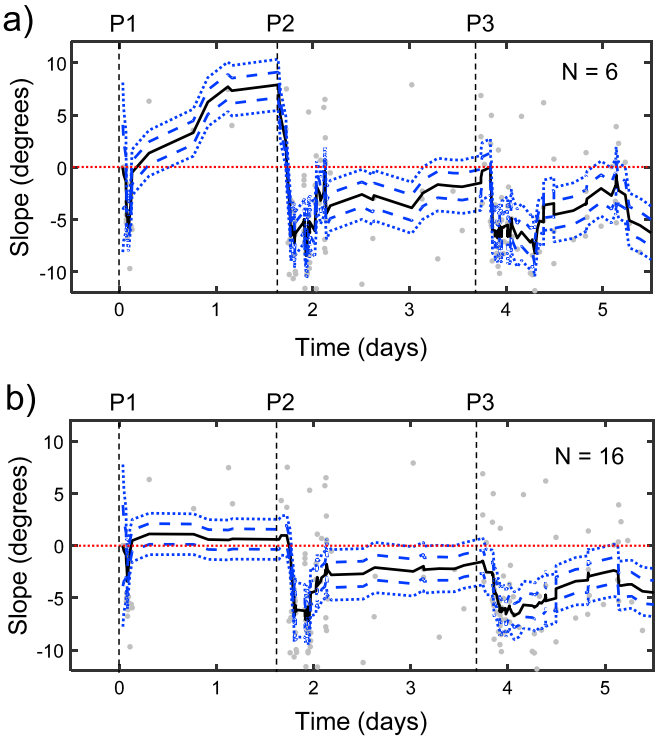

Figure 11. Detailed time evolution of the slope angle for the first three swarm phases of the 2008 earthquake swarm. The moving average of the slope (black solid line) is calculated for (a) 6 and (b) 16 successive earthquakes. The phase numbers P1–P3 of the swarm are indicated at the top of each panel. The gray dots show values for 249 selected earthquakes. The dashed and dotted blue lines show 1σ and 2σ uncertainties of moving averaging, where σ is the standard deviation (for details, see the text). The red dotted lines denote the slope of shear earthquakes.

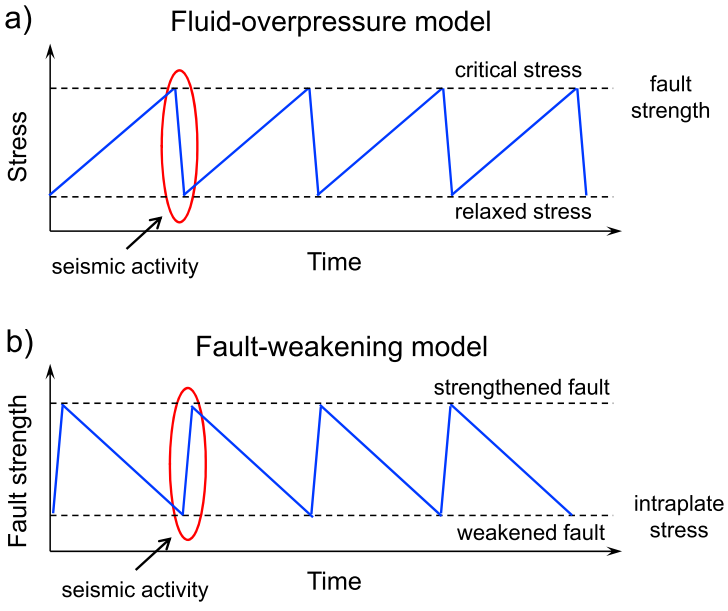

Figure 12. Earthquake swarm sequences. (a) The fluid-overpressure model. The seismic cycle is driven by gradually increased fluid pressure at the fault. If shear stress is critical and exceeds the fault strength, the earthquake occurs and stress is relaxed [*Kanamori and Brodsky*, 2004]. (b) The fault-weakening model. The seismic cycle is driven by a steady state circulation of fluids which gradually weakens the faults by chemical and hydrothermal fluid-rock interactions. If the fault strength reaches a critical value being lower than the intraplate stress, the seismicity is triggered, the pore volume in the eroded material is collapsed, and the fault strength is recovered.

mineral content of springs on the surface. Springs percolating through the local granitic and metamorphic host rock in the West Bohemia area show a typical enrichment in Na, Ca, Mg, Fe_2O_3, SiO_2, and HCO_3. Obviously, the dissolution of minerals leads to their deficit in the material inside fractures, to increasing porosity of the fault gauge, and to weakening of faults and fractures. A high porosity of a rock is manifested by anomalously low v_P/v_S ratio [*Vavryčuk*, 2011b; *Dahm and Fischer*, 2014] which is typical for geothermal and volcanic regions [*Lin and Shearer*, 2009].

If the fault strength (or equivalently the friction coefficient) lowers to a critical value due to the fault erosion and degradation by fluids, the seismicity is triggered. The predominant motion on fractures is shear being controlled by tectonic stress. However, a soft, highly porous material inside fractures is squeezed and compacting during shear failure. The fault is closing, and the fault strength recovers (see Figure 12b). Closing of the fault is associated with negative values of the slope angle and consequently with negative CLVD and ISO components. The fault compaction can temporarily increase fluid pressure in the focal area and initiate subsequent tensile faulting preferably along wing cracks which are distinctly inclined from the main active faults [*Dalguer et al.*, 2003; *Misra et al.*, 2009]. After recovering the whole focal zone, the seismicity stops. A new cycle begins by weakening the fault zone, gradually altered by migrating fluids.

The fault-weakening model is consistent not only with the observations of the 2008 swarm in West Bohemia but also with observations of the 1997 swarm for which the non-DC components of moment tensors were studied in detail [*Vavryčuk*, 2002]. The 1997 swarm activity began by the occurrence of faulting with non-negligible compressive motions manifested by negative CLVD and ISO components. In the second phase of the swarm, tensile earthquakes producing large CLVD and ISO components dominated. Tensile fracturing in the second swarm phase was likely due to a sudden pore pressure increase produced by fault compacting.

7. Discussion and Conclusions

The most decisive observations for recognizing the origin of a fluid-driven seismic activity are the non-DC components of moment tensors. Their accurate determination can resolve whether the activity is triggered by fluid overpressure or not. The presence of fluid overpressure is associated with shear-tensile faulting and manifested by positive ISO and CLVD components. However, if the ISO and CLVD components are negative, shear-compressive faulting is more likely to be present and the model with fluid overpressure is not applicable. Instead, the fault-weakening model is more suitable with the swarm activity being triggered by degradation of fault strength due to long-lasting fluid-rock interactions when fluids aggressively act on the rock and erode the fracture walls.

It is also possible that the seismic activity comprises both fluid-overpressure and fault-weakening mechanisms. If seismicity is triggered on an eroded fault, the fault gouge is compacting during fracture process and the fluid inside the fault is captured and loaded. Also, the Coulomb stress changes can pressurize fluids in the focal zone. Subsequently, sudden increase of fluid pressure can cause diffusion of fluids which might trigger other shear or shear-tensile fractures. This explains the success of the fluid diffusion model applied by *Parotidis et al.* [2003, 2005] to the 2000 earthquake swarm in West Bohemia. The involvement of fluid diffusion is also supported by the space-time distribution of the events during the swarm, which suggests an upward migration of seismicity with the first events occurring at the bottom and the latest events in the upper parts of the fault zone (see Figure 4). The diffusion process stops at depths of 5–6 km where a distinct layer with anomalous seismic properties is detected [*Alexandrakis et al.*, 2014; *Hrubcová et al.*, 2016; *Mullick et al.*, 2015].

Even though we speak about tensile or compressive faulting, the predominant faulting is always shearing. The slope angle of ±15° is small, and the displacement associated with opening or closing the fault is almost negligible compared to the slip magnitude on the fault. However, even small slope values affect distinctly the pattern of radiated waves and the resultant moment tensors inverted from them. For the station configuration in the West Bohemia region, the slope error is about ±4°, so the values of ±10°–15° can be detected reliably. The method is so robust because the DC and non-DC components are extremely sensitive to the slope and the DC is remarkable reduced even for small slope angles [*Vavryčuk*, 2011b]. For example, slope angle of 5° causes a reduction of the DC percentage by 15–20% depending on the v_P/v_S ratio at the focal zone.

An interesting and not fully solved question is why the majority of the earthquake swarms in West Bohemia is concentrated in a small Nový Kostel focal zone, while the other seismically active zones in West Bohemia are less active [*Fischer et al.*, 2014]. The key to understand this point is probably in presence of rocks particularly susceptible to degradation and erosion by fluids at the Nový Kostel focal zone at the seismogenic depths. Since the upper crust in West Bohemia displays a diverse geological pattern with presence of granites, granodiorites, amphibolites, mica schists, and gneisses as reported by *Chlupáčová et al.* [2003], *Mlčoch and Skácelová* [2009], and others, the rate of erosion of existing faults can significantly vary within the area. Additionally, the Nový Kostel focal zone lies at the intersection of the Eger Rift and Mariánské Lázně fault, so it might be a predisposed zone of weakness or a contact of two blocks of a different rheology [*Babuška et al.*, 2016].

The fault weakening mechanism should not be associated with any specific stress regime so it can be observed on strike-slip, normal, or reverse faults. Moreover, it might not be exclusively responsible not only for intraplate earthquake swarms but also for intraplate single earthquakes. Therefore, lowering fault strength and friction by long-lasting fluid erosion might be viewed as a physically plausible, general mechanism, which should be studied in future also for other types of intraplate seismicity and seismically active region.

Acknowledgments
We thank Martha Savage, Vladislav Babuška, and three anonymous reviewers for their detailed and helpful reviews and the WEBNET group for providing us with the WEBNET data. The acquisition and processing of data have been financed by the Ministry of Education, Youth and Sports project LM2015079. The work was supported by the Grant Agency of the Czech Republic grants 16-19751J and 17-19297S. The analyzed waveforms are available from the authors upon request (vv@ig.cas.cz). The moment tensors of the 249 selected earthquakes are provided in the supporting information. The percentages of the DC and non-DC components of moment tensors were calculated by using the open-access Matlab code MT-DECOMPOSITION (http://www.ig.cas.cz/mt-decomposition).

References

Alexandrakis, C., M. Caló, F. Bouchaala, and V. Vavryčuk (2014), Velocity structure and the role of fluids in the West Bohemia Seismic Zone, *Solid Earth*, *5*, 863–872, doi:10.5194/se-5-863-2014.

Alvizuri, C., and C. Tape (2016), Full moment tensors for small events ($M_w < 3$) at Uturuncu volcano, Bolivia, *Geophys. J. Int.*, *206*(3), 1761–1783.

Babuška, V., J. Plomerová, and T. Fischer (2007), Intraplate seismicity in the western Bohemian Massif (central Europe): A possible correlation with a paleoplate junction, *J. Geodyn.*, *44*, 149–159.

Babuška, V., B. Růžek, and D. Dolejš (2016), Origin of earthquake swarms in the western Bohemian Massif: Is the mantle CO_2 degassing, followed by the Cheb Basin subsidence, an essential driving force?, *Tectonophysics*, *668*, 42–51, doi:10.1016/j.tecto.2015.12.008.

Baig, A., and T. Urbancic (2010), Microseismic moment tensors: A path to understanding frac growth, *Lead. Edge*, *29*(3), 320–324.

Baisch, S., and H.-P. Harjes (2003), A model for fluid-injection-induced seismicity at the KTB, Germany, *Geophys. J. Int.*, *152*, 160–170.

Bak, P., and C. Tang (1989), Earthquakes as a self-organized critical phenomenon, *J. Geophys. Res.*, *94*, 15,635–15,637, doi:10.1029/JB094iB11p15635.

Bankwitz, P., G. Schneider, H. Kämpf, and E. Bankwitz (2003), Structural characteristics of epicentral areas in Central Europe: Study case Cheb Basin (Czech Republic), *J. Geodyn.*, *35*, 5–32.

Bouchaala, F., V. Vavryčuk, and T. Fischer (2013), Accuracy of the master-event and double-difference locations: Synthetic tests and application to seismicity in West Bohemia, Czech Republic, *J. Seismol.*, *17*(3), 841–859, doi:10.1007/s10950-013-9357-4.

Bräuer, K., H. Kämpf, S. Niedermann, G. Strauch, and J. Tesař (2008), Natural laboratory NW Bohemia: Comprehensive fluid studies between 1992 and 2005 used to trace geodynamic processes, *Geochem. Geophys. Geosyst.*, *9*, Q04018, doi:10.1029/2007GC001921.

Bräuer, K., H. Kämpf, and G. Strauch (2011), Monthly monitoring of gas and isotope compositions in the free gas phase at degassing locations close to the Nový Kostel focal zone in the western Eger Rift, Czech Republic, *Chem. Geol.*, *290*, 163–176.

Brudy, M., M. D. Zoback, K. Fuchs, F. Rummel, and J. Baumgärtner (1997), Estimation of the complete stress tensor to 8 km depth in the KTB scientific drill holes: Implications for crustal strength, *J. Geophys. Res.*, *102*, 18,453–18,475, doi:10.1029/96JB02942.

Byerlee, J. (1978), Friction of rocks, *Pure Appl. Geophys.*, *116*, 615–626.

Čermáková, H., and J. Horálek (2015), The 2011 West Bohemia (Central Europe) earthquake swarm compared with the previous swarms of 2000 and 2008, *J. Seismol.*, *19*, 899–913.

Červený, V. (2001), *Seismic Ray Theory*, 713 pp., Cambridge Univ. Press, Cambridge.

Chen, X., P. M. Shearer, and R. E. Abercrombie (2012), Spatial migration of earthquakes within seismic clusters in Southern California: Evidence for fluid diffusion, *J. Geophys. Res.*, *117*, B04301, doi:10.1029/2011JB008973.

Chlupáčová, M., Z. Skácelová, and V. Nehybka (2003), P-wave anisotropy of rocks from the seismic area in Western Bohemia, *J. Geodyn.*, *35*, 45–57.

Dahm, T., T. Fischer, and S. Hainzl (2008), Mechanical intrusion models and their implications for the possibility of magma-driven swarms in NW Bohemia region, *Stud. Geophys. Geod.*, *52*(4), 529–548.

Dahm, T., J. Horálek, and J. Šílený (2000), Comparison of absolute and relative moment tensor solutions for the January 1997 West Bohemia earthquake swarm, *Stud. Geophys. Geod.*, *44*, 233–250.

Dahm, T., and T. Fischer (2014), Velocity ratio variations in the source region of earthquake swarms in NW Bohemia obtained from arrival time double-differences, *Geophys. J. Int.*, *196*, 957–970.

Dalguer, L. A., K. Irikura, and J. D. Dieta (2003), Simulation of tensile crack generation by three-dimensional dynamic shear rupture propagation during an earthquake, *J. Geophys. Res.*, *108*(B3), 2144, doi:10.1029/2001JB001738.

Davi, R., and V. Vavryčuk (2012), Seismic network calibration for retrieving accurate moment tensors, *Bull. Seismol. Soc. Am.*, *102*(6), 2491–2506, doi:10.1785/0120110344.

Dorbath, L., N. Cuenot, A. Genter, and M. Frogneux (2009), Seismic response of the fractured and faulted granite of Soultz-sous-Forˆets (France) to 5 km deep massive water injections, *Geophys. J. Int.*, *177*, 653–675.

Fischer, T., and J. Horálek (2003), Space-time distribution of earthquake swarms in the principal focal zone of the NW Bohemia/Vogtland seismoactive region: Period 1985–2001, *J. Geodyn.*, *35*, 125–144.

Fischer, T., J. Horálek, J. Michálek, and A. Boušková (2010), The 2008 West Bohemia earthquake swarm in the light of the WEBNET network, *J. Seismol.*, *14*, 665–682.

Fischer, T., J. Horálek, P. Hrubcová, V. Vavryčuk, K. Bräuer, and H. Kämpf (2014), Intra-continental earthquake swarms in West-Bohemia and Vogtland: A review, *Tectonophysics*, *611*, 1–27, doi:10.1016/j.tecto.2013.11.001.

Floyd, J. S., J. C. Mutter, A. M. Goodliffe, and B. Taylor (2001), Evidence for fault weakness and fluid flow within an active low-angle normal fault, *Nature*, *411*, 779–783.
Foulger, G. R., B. R. Julian, D. P. Hill, A. M. Pitt, P. E. Malin, and E. Shalev (2004), Non-double-couple microearthquakes at Long Valley caldera, California, provide evidence for hydraulic fracturing, *J. Volcanol. Geotherm. Res.*, *132*, 45–71.
Frohlich, C. (1994), Earthquakes with non-double-couple mechanisms, *Science*, *264*, 804–809.
Gautheron, C., M. Moreira, and C. Allègre (2005), He, Ne and Ar composition of the European lithospheric mantle, *Chem. Geol.*, *217*, 97–112.
Geissler, W. H., H. Kämpf, R. Kind, K. Klinge, T. Plenefisch, J. Horálek, J. Zedník, and V. Nehybka (2005), Seismic structure and location of a CO_2 source in the upper mantle of the western Eger Rift, Central Europe, *Tectonics*, *24*, TC5001, doi:10.1029/2004TC001672.
Hainzl, S. (2004), Seismicity patterns of earthquake swarms due to fluid intrusion and stress triggering, *Geophys. J. Int.*, *159*, 1090–1096.
Hainzl, S., and Y. Ogata (2005), Detecting fluid signals in seismicity data through statistical earthquake modelling, *J. Geophys. Res.*, *110*, B05S07, doi:10.1029/2004JB003247.
Hainzl, S., T. Fischer, H. Čermáková, M. Bachura, and J. Vlček (2016), Aftershocks triggered by fluid intrusion: Evidence for the aftershock sequence occurred 2014 in West Bohemia/Vogtland, *J. Geophys. Res. Solid Earth*, *121*, 2575–2590, doi:10.1002/2015JB012582.
Heidbach, O., M. Tingay, A. Barth, J. Reinecker, D. Kurfeß, and B. Müller (2008), The World Stress Map database release 2008, doi:10.1594/GFZ.WSM.Rel2008 (last accessed February 2012).
Heinicke, J., T. Fischer, R. Gaupp, J. Götze, U. Koch, H. Konietzky, and K.-P. Stanek (2009), Hydrothermal alteration as a trigger mechanism for earthquake swarms: The Vogtland/NW Bohemia region as a case study, *Geophys. J. Int.*, *178*, 1–13.
Herrmann, R. B. (1979), FASTHYPO—A hypocenter location program, *Earthquake Notes*, *50*(2), 25–38, doi:10.1785/gssrl.50.2.25.
Hill, D. P. (1977), A model for earthquake swarms, *J. Geophys. Res.*, *82*, 1347–1352, doi:10.1029/JB082i008p01347.
Hirakawa, E., and S. Ma (2016), Dynamic fault weakening and strengthening by gouge compaction and dilatancy in a fluid-saturated fault zone, *J. Geophys. Res. Solid Earth*, *121*, 5988–6008, doi:10.1002/2015JB012509.
Horálek, J., T. Fischer, A. Boušková, and P. Jedlička (2000), The Western Bohemia/Vogtland region in the light of the WEBNET network, *Stud. Geophys. Geod.*, *44*(2), 107–125.
Horálek, J., Z. Jechumtálová, L. Dorbath, and J. Šílený (2010), Source mechanisms of micro-earthquakes induced in a fluid injection experiment at the HDR site Soultz-sous-Forets (Alsace) in 2003 and their temporal and spatial variations, *Geophys. J. Int.*, *181*(3), 1547–1565.
Hrubcová, P., V. Vavryčuk, A. Boušková, and J. Horálek (2013), Moho depth determination from waveforms of microearthquakes in the West Bohemia/Vogtland swarm area, *J. Geophys. Res. Solid Earth*, *118*, 120–137, doi:10.1029/2012JB009360.
Hrubcová, P., V. Vavryčuk, A. Boušková, and M. Bohnhoff (2016), Shallow crustal discontinuities inferred from waveforms of microearthquakes: Method and application to KTB drill site and West Bohemia swarm area, *J. Geophys. Res. Solid Earth*, *121*, 881–902, doi:10.1002/2015JB012548.
Julian, B. R., A. D. Miller, and G. R. Foulger (1998), Non-double-couple earthquakes 1: Theory, *Rev. Geophys.*, *36*, 525–549.
Kanamori, H., and E. E. Brodsky (2004), The physics of earthquakes, *Rep. Prog. Phys.*, *67*, 1429–1496.
Kravanja, S., F. Batini, A. Fiordelist, and G. F. Panza (2000), Full moment tensor retrieval from waveform inversion in the Larderello geothermal area, *Pure Appl. Geophys.*, *157*, 1379–1392.
Kuehn, D., and V. Vavryčuk (2013), Determination of full moment tensors of microseismic events in a very heterogeneous mining environment, *Tectonophysics*, *589*, 33–43.
Lachenbruch, A. H. (1980), Frictional heating, fluid pressure, and the resistance to fault motion, *J. Geophys. Res.*, *85*, 6097–6112, doi:10.1029/JB085iB11p06097.
Lin, G., and P. Shearer (2009), Evidence for water-filled cracks in earthquake source regions, *Geophys. Res. Lett.*, *36*, L17315, doi:10.1029/2009GL039098.
Málek, J., J. Janský, and J. Horálek (2000), Layered velocity models of the western Bohemia region, *Stud. Geophys. Geod.*, *44*(4), 475–490.
Maxwell, S. C., J. Rutledge, R. Jones, and M. Fehler (2010), Petroleum reservoir characterization using downhole microseismic monitoring, *Geophysics*, *75*, A129–A137.
Michael, A. J. (1984), Determination of stress from slip data: Faults and folds, *J. Geophys. Res.*, *89*, 11,517–11,526.
Michael, A. J. (1987), Use of focal mechanisms to determine stress: A control study, *J. Geophys. Res.*, *92*(B1), 357–368.
Miller, S. A., C. Collettini, L. Chiaraluce, M. Cocco, M. Barchi, and B. J. P. Kaus (2004), Aftershocks driven by a high pressure CO_2 source at depth, *Nature*, *427*, 724–727.
Misra, S., N. Mandal, R. Dhar, and C. Chakraborty (2009), Mechanisms of deformation localization at the tips of shear fractures: Findings from analogue experiments and field evidence, *J. Geophys. Res.*, *114*, B04204, doi:10.1029/2008JB005737.
Mlčoch, B., and Z. Skácelová (2009), Digital elevation model of the crystalline basement in the Cheb and Sokolov Basin areas (Western Bohemia, Central Europe), *Z. Geol. Wiss Berlin*, *37*(3), 145–152.
Mogi, K. (1963), Some discussions on aftershocks, foreshocks and earthquake swarms—The fracture of a semi-infinite body caused by an inner stress origin and its relation to the earthquake phenomena, *Bull. Earthquake Res. Inst. Tokyo Univ.*, *41*, 615–658.
Mullick, N., S. Buske, P. Hrubcová, B. Růžek, S. Shapiro, P. Wigger, and T. Fischer (2015), Seismic imaging of the geodynamic activity at the western Eger Rift in central Europe, *Tectonophysics*, *647-648*, 105–111, doi:10.1016/j.tecto.2015.02.010.
Nayak, A., and D. Dreger (2014), Moment tensor inversion of seismic events associated with the sinkhole at Napoleonville salt dome, Louisiana, *Bull. Seismol. Soc. Am.*, *104*(4), 1763–1776.
Panza, G. F., and A. Sarao (2000), Monitoring volcanic and geothermal areas by full seismic moment tensor inversion: Are non-double-couple components always artefacts of modelling?, *Geophys. J. Int.*, *145*, 319–335.
Parotidis, M., E. Rothert, and S. A. Shapiro (2003), Pore-pressure diffusion: A possible triggering mechanism for the earthquake swarms 2000 in Vogtland/NW-Bohemia, central Europe, *Geophys. Res. Lett.*, *30*(20), 2075, doi:10.1029/2003GL018110.
Parotidis, M., S. A. Shapiro, and E. Rothert (2005), Evidence for triggering of the Vogtland swarms 2000 by pore pressure diffusion, *J. Geophys. Res.*, *110*, B05S10, doi:10.1029/2004JB003267.
Pesicek, J. D., J. Sileny, S. G. Prejean, and C. H. Thurber (2012), Determination and uncertainty of moment tensors for microearthquakes at Okmok volcano, Alaska, *Geophys. J. Int.*, *190*(3), 1689–1709.
Phillips, W. S., T. D. Fairbanks, J. T. Rutledge, and D. W. Anderson (1998), Induced microearthquake patterns and oil-producing fracture systems in the Austin chalk, *Tectonophysics*, *289*, 153–169.
Rice, J. R., J. W. Rudnicki, and J. D. Platt (2014), Stability and localization of rapid shear in fluid-saturated fault gouge: 1. Linearized stability analysis, *J. Geophys. Res. Solid Earth*, *119*, 4311–4333, doi:10.1002/2013JB010710.
Rubin, A. M., D. Gillard, and J. L. Got (1998), A reinterpretation of seismicity associated with the January 1983 dike intrusion at Kilauea volcano, Hawaii, *J. Geophys. Res.*, *103*, 10,003–10,015, doi:10.1029/97JB03513.

Rudajev, V., and J. Šílený (1985), Seismic events with non-shear component 2, rock bursts with implosive source component, *Pure Appl. Geophys.*, *123*(1), 17–25.
Scholz, C. H. (2002), *The Mechanics of Earthquakes and Faulting*, 471 pp., Cambridge Univ. Press, Cambridge, U. K.
Shapiro, S. A. (2015), *Fluid-Induced Seismicity*, 289 pp., Cambridge Univ. Press, Cambridge, U. K.
Shapiro, S. A., and C. Dinske (2009), Scaling of seismicity induced by nonlinear fluid-rock interaction, *J. Geophys. Res.*, *114*, B09307, doi:10.1029/2008JB006145.
Shelly, D. R., D. P. Hill, F. Massin, J. Farrell, R. B. Smith, and T. Taira (2013), A fluid-driven earthquake swarm on the margin of the Yellowstone Caldera, *J. Geophys. Res. Solid Earth*, *118*, 4872–4886, doi:10.1002/jgrb.50362.
Sibson, R. H. (1973), Interaction between temperature and pore-fluid pressure during earthquake faulting—A mechanism for partial or total stress relief, *Nature*, *243*, 66–68.
Sibson, R. H. (1996), Structural permeability of fluid-driven fault-fracture meshes, *J. Struct. Geol.*, *18*, 1031–1042.
Sibson, R. H. (2000), Fluid involvement in normal faulting, *J. Geodyn.*, *29*(3–5), 469–499.
Šílený, J. (2009), Resolution of non-double-couple mechanisms: Simulation of hypocenter mislocation and velocity structure mismodelling, *Bull. Seismol. Soc. Am.*, *99*, 2265–2272.
Šílený, J., P. Campus, and G. F. Panza (1996), Seismic moment tensor resolution by waveform inversion of a few local noisy records. 1. Synthetic tests, *Geophys. J. Int.*, *126*, 605–619.
Šílený, J., and A. Milev (2008), Source mechanism of mining induced seismic events—Resolution of double couple and non double couple models, *Tectonophysics*, *456*(1–2), 3–15.
Šílený, J., and V. Vavryčuk (2000), Approximate retrieval of the point source in anisotropic media: Numerical modelling by indirect parameterization of the source, *Geophys. J. Int.*, *143*, 700–708, doi:10.1046/j.1365-246X.2000.00256.x.
Šílený, J., and V. Vavryčuk (2002), Can unbiased source be retrieved from anisotropic waveforms by using an isotropic model of the medium?, *Tectonophysics*, *356*, 125–138, doi:10.1016/S0040-1951(02)00380-3.
Sleep, N. H., and M. L. Blanpied (1992), Creep, compaction and the weak rheology of major faults, *Nature*, *359*, 687–692.
Špičák, A., and J. Horálek (2001), Possible role of fluids in the process of earthquake swarm generation in the West Bohemia/Vogtland seismoactive region, *Tectonophysics*, *336*, 151–161.
Stierle, E., V. Vavryčuk, J. Šílený, and M. Bohnhoff (2014), Resolution of non-double-couple components in the seismic moment tensor using regional networks: 1. A synthetic case study, *Geophys. J. Int.*, *196*(3), 1869–1877, doi:10.1093/gji/ggt502.
Suto, Y., L. H. Liu, N. Yamasaki, and T. Hashida (2007), Initial behavior of granite in response to injection of CO_2-saturated fluid, *Appl. Geochem.*, *22*, 202–218.
Trifu, C.-I., and V. Shumila (2010), Microseismic monitoring of a controlled collapse in field II at Ocnele Mari, Romania, *Pure Appl. Geophys.*, *167*(1–2), 27–42.
Vavryčuk, V. (1993), Crustal anisotropy from local observations of shear-wave splitting in West Bohemia, Czech Republic, *Bull. Seismol. Soc. Am.*, *83*, 1420–1441.
Vavryčuk, V. (2002), Non-double-couple earthquakes of January 1997 in West Bohemia, Czech Republic: Evidence of tensile faulting, *Geophys. J. Int.*, *149*, 364–373.
Vavryčuk, V. (2005), Focal mechanisms in anisotropic media, *Geophys. J. Int.*, *161*, 334–346, doi:10.1111/j.1365-246X.2005.02585.x.
Vavryčuk, V. (2011a), Principal earthquakes: Theory and observations for the 2008 West Bohemia swarm, *Earth Planet. Sci. Lett.*, *305*, 290–296.
Vavryčuk, V. (2011b), Tensile earthquakes: Theory, modeling, and inversion, *J. Geophys. Res.*, *116*, B12320, doi:10.1029/2011JB008770.
Vavryčuk, V. (2014), Iterative joint inversion for stress and fault orientations from focal mechanisms, *Geophys. J. Int.*, *199*(1), 69–77, doi:10.1093/gji/ggu224.
Vavryčuk, V. (2015), Moment tensor decompositions revisited, *J. Seismol.*, *19*(1), 231–252, doi:10.1007/s10950-014-9463-y.
Vavryčuk, V., M. Bohnhoff, Z. Jechumtálová, P. Kolář, and J. Šílený (2008), Non-double-couple mechanisms of micro-earthquakes induced during the 2000 injection experiment at the KTB site, Germany: A result of tensile faulting or anisotropy of a rock?, *Tectonophysics*, *456*, 74–93.
Vavryčuk, V., F. Bouchaala, and T. Fischer (2013), High-resolution fault image from accurate locations and focal mechanisms of the 2008 swarm earthquakes in West Bohemia, Czech Republic, *Tectonophysics*, *590*, 189–195, doi:10.1016/j.tecto.2013.01.025.
Waite, G.P., and R. B. Smith (2002), Seismic evidence for fluid migration accompanying subsidence of the Yellowstone Caldera, *J. Geophys. Res.*, *107*(B9), 2177, doi:10.1029/2001JB000586.
Waldhauser, F., and W. L. Ellsworth (2000), A double-difference location algorithm: Method and application to the Northern Hayward Fault, California, *Bull. Seismol. Soc. Am.*, *78*, 1353–1368.
Weinlich, F. H., K. Bräuer, H. Kämpf, G. Strauch, J. Tesar, and S. M. Weise (1999), An active subcontinental mantle volatile system in the western Eger Rift, Central Europe: Gas flux, isotopic (He, C, and N) and compositional fingerprints, *Geochim. Cosmochim. Acta*, *63*, 3653–3671.
Whidden, K. M., and K. L. Pankow (2016), Shear waves from isotropically dominated sources: Comparison of the 2013 Rudna, Poland, and 2007 Crandall Canyon, Utah, mine collapses, *Bull. Seismol. Soc. Am.*, *106*(2), 799–805.
Yamashita, T. (1999), Pore creation due to fault slip in a fluid-permeated fault zone and its effect on seismicity: Generation mechanism of earthquake swarm, *Pure Appl. Geophys.*, *155*, 625–647.
Yoshida, K., A. Hasegawa, and T. Yoshida (2016), Temporal variation of frictional strength in an earthquake swarm in NE Japan caused by fluid migration, *J. Geophys. Res. Solid Earth*, *121*, 5953–5965, doi:10.1002/2016JB013022.
Zhao, L.-S., and D. V. Helmberger (1994), Source estimation from broadband regional seismograms, *Bull. Seismol. Soc. Am.*, *84*(1), 91–104.